Received: 17 March 2026 | Revised: 13 July 2026 | Accepted: 18 July 2026 | Published online: 11 August 2026

RESEARCH ARTICLE

Green and Low-Carbon Economy
2026, Vol. 00(00) 1–17
DOI: 10.47852/bonviewGLCE62029684

BON VIEW PUBLISHING

Sentinel-5P Evidence for Low-Carbon Energy Planning and Arctic Air-Quality Resilience in Yukon and Alaska

Matthew McCarthy[1], Davoud Ghahremanlou[1,*] and Amir Ghahremanlou[2]

[1] *Faculty of Business Administration, Memorial University of Newfoundland, Canada*

[2] *Department of Civil Engineering, Islamic Azad University (Science and Research Branch), Iran*

Abstract: Remote Arctic and sub-Arctic communities face intersecting pressures from rapid climate change, high energy costs, combustion-based heating, and sparse environmental monitoring. In Yukon and Alaska, these conditions make air quality not only a public-health concern but also an important consideration for low-carbon energy planning and climate resilience. This study develops a six-year (2019–2024), paired-jurisdiction framework using Sentinel-5P TROPOMI carbon monoxide (CO) and nitrogen dioxide (NO_2) observations to provide screening-level evidence for Arctic air-quality management and cleaner energy transitions. Satellite data were quality-screened and processed in Google Earth Engine and Python and then analyzed through annual, seasonal, and monthly aggregation, hotspot mapping, and Mann–Kendall and Seasonal Mann–Kendall trend tests. Results reveal a persistent jurisdictional split. CO remained consistently higher in Alaska than in Yukon (0.0296–0.0340 vs 0.0271–0.0310 mol m^{-2}), while NO_2 was substantially higher in Yukon than in Alaska (4.65×10^{-5}–5.18×10^{-5} vs 3.81×10^{-6}–5.05×10^{-6} mol m^{-2}). Seasonal contrasts were stable, with Alaska exceeding Yukon for CO in all seasons and Yukon exceeding Alaska for NO_2 by roughly an order of magnitude. Monthly Seasonal Mann–Kendall analysis detected modest but significant CO declines in both jurisdictions, at about 1.5% per year, whereas NO_2 showed no significant trend. Recurrent hotspots were concentrated in interior Alaska and northern Yukon for CO and along the Anchorage–Kenai corridor and northern Yukon for NO_2. These findings suggest that Sentinel-5P can support low-carbon energy planning, smoke-season preparedness, inversion-time response, and equity-centered Arctic resilience in sparsely monitored northern regions.

Keywords: Sentinel-5P, low-carbon energy planning, Arctic resilience

1. Introduction

The Arctic is warming at roughly four times the global average, intensifying environmental, infrastructural, and social pressures across high-latitude regions [1]. Recent assessments continue to document unprecedented Arctic change. The Arctic Report Card 2025 identifies the 2024–2025 period as the warmest Arctic year on record since at least 1900, accompanied by record precipitation, continued sea-ice decline, accelerating permafrost-related impacts, and increasing environmental risks to northern communities and infrastructure [2]. Continued ice loss, permafrost degradation, changing circulation, and shifting wildfire regimes are reshaping ecological and socioeconomic systems within the Arctic and beyond [3, 4]. In remote northern jurisdictions, these changes have immediate implications not only for environmental quality and public health but also for the affordability, reliability, and sustainability of local energy systems. Many Arctic and sub-Arctic communities face a difficult combination of high energy costs, dependence on combustion-based heating or diesel-powered electricity, sparse service infrastructure, and limited environmental monitoring. In this context, improving air-quality intelligence is not only a health imperative but also an increasingly important component of low-carbon energy planning and climate resilience.

Within this rapidly changing system, carbon monoxide (CO) and nitrogen dioxide (NO_2) are especially informative pollutants. NO_2 is short-lived and closely linked to local combustion, transport activity, and concentrated emission sources, while CO persists longer, integrates wildfire and transport signals, and influences oxidant chemistry as well as downwind ozone and aerosol formation [5, 6]. Their relevance is heightened in Arctic and sub-Arctic settings, where winter inversions, heating fuels, mobile diesel use, and increasingly severe wildfire seasons elevate exposure risks, strain health services, and complicate efforts to build cleaner and more resilient energy systems. These burdens often fall disproportionately on remote and Indigenous communities, where healthcare access may be limited and the cost of conventional energy remains high. Accordingly, air-quality monitoring in such regions is no longer only an atmospheric-chemistry problem;

*Corresponding author: Davoud Ghahremanlou, Faculty of Business Administration, Memorial University of Newfoundland, Canada. Email: dghahremanlo@mun.ca

it is also a governance, equity, and infrastructure-planning challenge tied to broader green and low-carbon transition goals.

Yet routine ground-based monitoring remains sparse across northern regions such as Yukon (YT) and Alaska (AK), largely because of logistical, climatic, and financial constraints. Satellite remote sensing therefore offers an important opportunity to support decision-making at jurisdictional scale, particularly in large and sparsely monitored regions where repeated spatial coverage can strengthen climate resilience planning and reduce the cost of conventional monitoring approaches [7–9]. Sentinel-5P TROPOMI, with nadir resolution of approximately 5.5 × 3.5 km^2, can reveal stable contrasts, recurrent hotspots, and seasonality across large, remote territories where station networks remain thin. When paired jurisdictions are examined under broadly similar latitude and synoptic conditions, satellite observations can provide policy-relevant evidence while reducing some confounding associated with wider pan-Arctic comparisons [7, 8]. Such evidence can help identify where smoke preparedness, inversion-time response, clean-heating upgrades, or diesel-to-hybrid micro-grid interventions may yield the greatest co-benefits for public health, resilience, and energy transition.

Despite growing attention to Arctic air quality, three limitations still hinder the translation of satellite observations into decision-ready evidence for low-carbon planning and societal resilience in data-sparse regions. First, scope fragmentation: prior multi-year studies often examine a single pollutant or a single geographic regime, such as NO_2 from OMI or TROPOMI in broad hemispheric analyses, or CO from MOPITT or AIRS over parts of the Arctic and boreal domain [10–14]. While valuable, including recent Sentinel-5P studies of Arctic atmospheric composition and pollutant dynamics [7, 15], such investigations provide limited insight into how adjacent northern jurisdictions differ under distinct source mixes, boundary-layer behavior, infrastructure contexts, and low-carbon transition priorities. Recent Arctic assessments and monitoring programs have increasingly emphasized the need for spatially explicit environmental intelligence capable of supporting adaptation, resilience, and low-carbon transition planning in rapidly changing northern regions [2, 16]. However, relatively few satellite-based investigations have adopted paired-jurisdiction (bilateral comparison) designs that directly compare neighboring Arctic regions under broadly similar climatic conditions while evaluating implications for operational decision-making. Second, aggregation bias: pan-Arctic syntheses often obscure jurisdiction-scale contrasts that matter for place-based planning, including the timing of inversion response, smoke-season readiness, or prioritization of cleaner local energy systems [17, 18], whereas spatially explicit approaches are better suited to identifying context-specific interventions and infrastructure priorities [19]. Third, validation asymmetry: although satellite retrievals are increasingly mature, formal comparisons that keep atmospheric columns analytically distinct from surface inventories and sparse ground data remain uncommon precisely where monitoring is thinnest [20–22]. Additional challenges arise in high-latitude environments where snow and ice surface reflectance, persistent cloud cover, low solar-elevation angles, and seasonal darkness can influence retrieval sensitivity and uncertainty. Recent high-latitude TROPOMI studies show that Arctic and sub-Arctic applications require particular caution because valid NO_2 retrieval availability can vary strongly with season, cloud conditions, surface reflectance, and solar geometry. For example, work over Norway demonstrated substantial spatiotemporal variability in valid TROPOMI NO_2 observations [23], while studies over Finland showed that translating TROPOMI NO_2 columns into surface-level concentrations requires explicit attention to boundary-layer mixing and local meteorology [16]. These studies not only support the use of Sentinel-5P as a complementary monitoring tool in northern regions but also reinforce the need to interpret column differences as quality-screened atmospheric evidence rather than direct surface exposure or emissions estimates. Although recent Sentinel-5P studies have demonstrated strong utility for Arctic monitoring, these factors remain important considerations when interpreting pollutant distributions and temporal variability in northern regions [15, 24]. This weakens operational uptake, especially for agencies seeking auditable, transferable workflows that connect atmospheric evidence with environmental management and infrastructure planning.

These gaps matter because the stakes are rising. AK faces substantial projected infrastructure damages linked to permafrost thaw [25], while YT has already experienced major warming and is expected to undergo further climatic disruption during this century [26]. Such conditions are likely to intensify stagnation events, alter wildfire regimes, and reshape atmospheric chemistry [27–29]. At the same time, remote communities must navigate the dual challenge of reducing dependence on high-emission energy systems while protecting residents from smoke, inversion-driven pollution episodes, and uneven exposure burdens, a pattern consistent with broader low-carbon transition research emphasizing the importance of infrastructure, coordination, and implementation capacity in moving from transition ambition to operational delivery [30]. This challenge is especially acute in isolated northern communities, where diesel dependence, high delivered fuel costs, limited grid connectivity, and difficult logistics constrain decarbonization pathways and increase the value of targeted evidence for hybrid micro-grid planning, clean heating, and renewable-energy integration. There is therefore a strong need for evidence frameworks that are scientifically transparent, spatially comprehensive, and directly relevant to low-carbon adaptation and energy-system decision-making.

This study addresses that need through a six-year (2019–2024), bilateral comparison assessment of YT and AK using Sentinel-5P observations of CO and NO_2. The paired design helps hold latitude and broad synoptic setting relatively constant while highlighting how source structure, boundary-layer processes, and seasonal forcing shape jurisdiction-specific air-quality regimes. The study is designed not only to characterize spatiotemporal pollutant contrasts but also to translate those contrasts into evidence relevant to cleaner heating, assessment of hybrid micro-grid opportunities, smoke preparedness, and equity-centered Arctic resilience. Specifically, the objectives are to (1) quantify annual, seasonal, and monthly contrasts in CO and NO_2 column densities and assess detectable trends, (2) identify recurrent hotspots and transboundary corridors using a transparent and auditable spatial workflow, and (3) evaluate the practical usefulness of satellite evidence through comparisons with emission inventories and limited ground data while preserving conceptual separation between atmospheric columns and surface domains.

The principal contribution of this study is the development of an integrated decision-support framework for sparsely monitored Arctic jurisdictions. Existing studies have commonly applied Sentinel-5P to characterize pollutant distributions within individual regions or across broad pan-Arctic domains. In contrast, this study combines a paired-jurisdiction comparison, dual-pollutant assessment, season-aware temporal analysis, hotspot persistence mapping, and policy translation within a single reproducible workflow specifically designed to support low-carbon planning and climate resilience decision-making in remote northern systems. The remainder of the paper proceeds as follows. Section 2 describes the study area, data, and analytical workflow. Section 3 presents annual, seasonal, monthly, spatial, comparative, and trend results. Section 4 interprets the findings in relation to source dynamics, resilience, and policy action, with a specific focus on low-carbon planning implications. Section 5 concludes with key findings, limitations, and recommendations for future research and decision-making in high-latitude regions. In doing so, the paper positions satellite-derived air-quality evidence as a practical input to low-carbon transition planning in climate-sensitive, sparsely monitored northern systems.

2. Materials and Methods

CO and NO_2 column densities from Sentinel-5P were analyzed over 2019–2024 to examine air-quality dynamics relevant to low-carbon energy planning and Arctic resilience in YT and AK. The study period captures a policy-relevant window in which both Canada and the United States advanced major climate and emissions-reduction commitments, while northern regions continued to experience increasing climate stress, wildfire risk, and pressure to improve the reliability and sustainability of local energy systems [31, 32]. This timeframe therefore provides an appropriate basis for evaluating how satellite-derived air-quality evidence can support decision-making under active transition conditions.

Sentinel-5P was selected because its spatial resolution is well suited to monitoring large and remote northern jurisdictions where conventional ground networks remain sparse. Satellite retrievals, expressed as total column density (mol m^{-2}), provide an elevation-independent basis for comparing atmospheric burdens across complex terrain. Data extraction and screening were performed in Google Earth Engine, processing and aggregation were conducted in Python 3.13.0, and spatial hotspot analysis was completed in ArcGIS 10.8. Annual, seasonal, and monthly composites were produced to identify persistent contrasts, seasonal windows, and recurrent high-burden areas. To support operational interpretation, annual satellite averages were also compared empirically with jurisdiction-level emission inventories from Environment and Climate Change Canada and the US Environmental Protection Agency (EPA), while maintaining a clear distinction between atmospheric column observations and surface emission data [33].

This multi-scale design was selected to move beyond descriptive mapping toward decision-relevant evidence. In particular, the framework is intended to identify where monitoring gaps, smoke-season readiness, clean-heating strategies, and diesel-to-hybrid micro-grid upgrades may merit higher priority in remote northern settings. Complementary Sentinel-2/Sentinel-5P fusion approaches can eventually support more localized NO_2 applications where sufficient surface references exist [34]. Uncertainty was summarized using mean values, standard deviations, and 95% confidence intervals (CIs). Monotonic trends were evaluated using the non-parametric Mann–Kendall (MK) test for annual series and the Seasonal Mann–Kendall (SMK) test for monthly series, with Sen's slope used to estimate trend magnitude. These methods were selected because atmospheric pollutant datasets frequently exhibit non-normal distributions, seasonal variability, and potential outliers associated with wildfire events and episodic transport processes. Compared with conventional parametric approaches, MK and SMK tests provide robust trend assessment without requiring assumptions of normality or linearity, making them well suited to environmental time-series analysis in Arctic and sub-Arctic regions.

2.1. Study area

YT is a northern Canadian territory with a population of approximately 47,000 and an area of about 482,443 km^2, while AK, immediately to its west, is a US state with a population of about 740,000 and an area of about 1,717,856 km^2 (Figure 1) [35, 36]. Together, they form a useful, paired study system for examining adjacent high-latitude jurisdictions that share broad climatic exposure while differing in settlement structure, industrial activity, and energy-use profiles.

Both jurisdictions are environmentally and socially important in the context of Arctic transition. Indigenous populations account for a substantial share of residents, approximately 22.3% in YT and 15.7% in AK [35, 36], highlighting the importance of environmental justice, culturally appropriate governance, and data sovereignty in monitoring and intervention design [37]. Many communities across the region face high energy costs, long supply chains, dependence on combustion-based heating or diesel-powered systems, and limited access to healthcare and environmental monitoring. These conditions increase vulnerability to pollution episodes associated with wildfire smoke, winter inversions, and local combustion sources.

The study area is influenced by both natural and anthropogenic emissions, including forest fires, transport activity, industrial operations, and heating-related combustion. Strong seasonality and frequent wintertime temperature inversions can intensify pollutant accumulation, especially in valleys, basins, and poorly ventilated corridors [38]. These dynamics make YT and AK particularly suitable for evaluating whether satellite-derived CO and NO_2 fields can reveal not only atmospheric contrasts but also planning-relevant spatial patterns linked to cleaner energy interventions and resilience priorities in rapidly changing Arctic and sub-Arctic systems. The paired YT–AK comparison is therefore not intended to imply that the two jurisdictions are identical. Rather, it provides a controlled regional contrast between adjacent high-latitude systems that share broad Arctic/sub-Arctic climatic exposure while differing in settlement structure, industrial activity, energy systems, and monitoring capacity. This design reduces some confounding associated with pan-Arctic comparisons while preserving the jurisdiction-level differences that are most relevant for policy and infrastructure planning.

2.2. Data compilation methods

Assessing transboundary air quality between YT and AK requires spatially consistent pollutant information across large, sparsely monitored areas. Sentinel-5P data for 2019–2024 were retrieved in Google Earth Engine using the collections COPERNICUS/S5P/NRTI/L3_CO and COPERNICUS/S5P/NRTI/L3_NO_2. Ground-based comparison data were compiled for 2020–2023 from YT sources and the US EPA for AK [35]. The shorter ground-data window was used to reduce the influence of anomalous reporting gaps and early-pandemic inconsistencies, while the satellite analysis retained the full 2019–2024 period to preserve continuity in atmospheric signal assessment.

To ensure data quality, retrievals were screened using qa_value $\geq$ 0.5, cloud fraction $<$ 0.6, and solar-zenith angle $\leq$ 70°, with all other observations discarded prior to aggregation. In high-latitude winter conditions, the combined application

Figure 1
Geographic location of the study area: (a) global context, (b) Yukon, and (c) Alaska

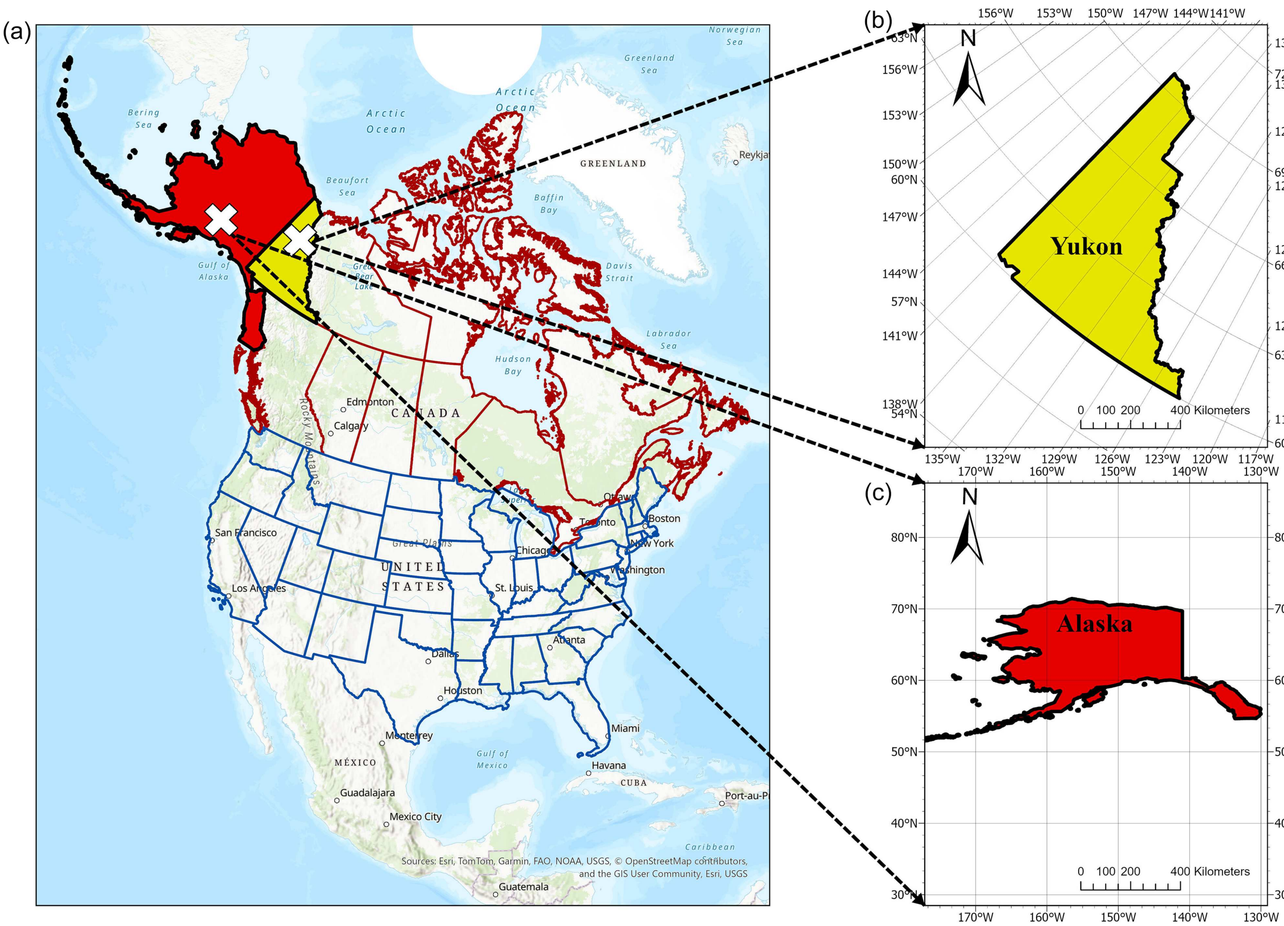

of quality filters may substantially reduce the number of valid observations. In particular, portions of YT exhibited no valid December NO_2 retrievals after screening because low solar-elevation angles and persistent cloud cover frequently prevented observations from meeting the adopted quality criteria. These missing observations were retained as missing values rather than interpolated to preserve methodological transparency. Although Sentinel-5P spatial resolution varies across the swath and becomes coarser toward off-nadir viewing geometries, the quality-assurance filtering applied in this study was designed to minimize retrieval artifacts and maintain comparability across observations. Observation-weighted averaging was then applied using pixel counts as weights, and monthly and annual composites were calculated from valid pixels using area-weighted averaging. This approach improves comparability across time and space while remaining transparent and reproducible [39].

Satellite-derived annual averages were compared empirically with jurisdiction-level emission inventories as a unit-independent concordance assessment rather than a validation exercise. Satellite column densities and inventory-based emissions represent different physical quantities and are influenced by distinct processes, including atmospheric transport, boundary-layer dynamics, chemical transformation, reporting methodologies, and temporal aggregation. Consequently, the objective was not to establish predictive relationships or infer emissions from satellite observations but rather to evaluate whether broad directional patterns were consistent across independent evidence streams. Given the limited number of annual observations and the differing physical meaning of the datasets, the analysis was interpreted as an exploratory concordance screen rather than a formal regression-based model. These inventories should not be interpreted as ground-monitoring observations. Rather, they represent independently compiled emissions estimates that were used solely as a complementary evidence stream for broad directional comparison with satellite-derived atmospheric column measurements. This workflow was selected to support both scientific interpretation and practical policy use. By combining quality-assured satellite compositing, hotspot mapping, and limited inventory cross-checking, the approach enables identification of stable burdens, recurrent high-risk corridors, and seasonal intervention windows relevant to smoke response, clean-heating strategies, and low-carbon infrastructure planning in remote northern regions. For hotspot visualization and interpretation, annual pollutant concentrations were classified into five categories (very low, low, moderate, high, and very high) using the Jenks Natural Breaks method in ArcGIS 10.8. This classification approach minimizes within-class variance while maximizing between-class differences, making it well suited to identifying meaningful spatial clusters and recurrent burden patterns in heterogeneous environmental datasets. Classification thresholds were calculated separately for CO and NO_2 based on the distribution of annual concentrations for each mapped year. A similar hotspot-screening framework combining Sentinel-5P observations with Jenks-based classification has recently been applied to continental-scale methane assessment in Australia, demonstrating its usefulness for identifying persistent environmental burden zones and priority areas for follow-up investigation [40].

Because this study is designed as an exploratory, screening-level assessment, the workflow is intended to identify persistent atmospheric patterns and priority areas for follow-up rather than to provide source attribution or direct exposure estimation. Sentinel-5P column observations, jurisdiction-level inventories, and limited surface datasets represent different physical domains and therefore cannot be interpreted as one-to-one validation sources. Accordingly, the results are used to support directional interpretation, hotspot screening, and monitoring prioritization, while stronger attribution would require expanded ground observations, vertical-profile information, inverse modeling, or chemical transport modeling.

3. Results

3.1. Annual temporal trends in pollutant concentrations

Table 1 and its companion figure summarize annual jurisdiction-wide means of carbon monoxide (CO) and nitrogen dioxide (NO_2) column density (mol m^{-2}) from 2019 to 2024 for AK and YT. CO remains consistently higher in AK than YT each year, spanning 0.0296-0.0340 mol m^{-2} in AK versus 0.0271-0.0310 mol m^{-2} in YT. Over the full period, the six-year mean (±SD) CO is 0.03220 ± 0.00149 mol m^{-2} in AK and 0.02965 ± 0.00143 mol m^{-2} in YT, with corresponding 95% confidence intervals of 0.03064-0.03376 mol m^{-2} (AK) and 0.02815-0.03115 mol m^{-2} (YT). By contrast, NO_2 is consistently higher in YT than AK. Annual NO_2 means range from 4.65×10^{-5} to 5.18×10^{-5} mol m^{-2} in YT versus 3.81×10^{-6} to 5.05×10^{-6} mol m^{-2} in AK. Aggregated across years, the six-year mean (±SD) NO_2 is 4.88 × 10–5 ± 1.72×10^{-6} mol m^{-2} in YT and 4.32×10^{-6} ± 4.58×10^{-7} mol m^{-2} in AK, with 95% confidence intervals of 4.70×10^{-5}-5.06×10^{-5} mol m^{-2} (YT) and 3.84×10^{-6}-4.80×10^{-6} mol m^{-2} (AK). Year-to-year CO variability is modest in both jurisdictions, and the NO_2 series shows a stable YT-AK separation with comparatively small annual fluctuations, underscoring the ability of Sentinel-5P to resolve persistent regional contrasts across remote northern jurisdictions. Because NO_2 retrievals in high-latitude environments are sensitive to solar geometry, cloud screening, snow/ice reflectance, and boundary-layer structure, the Yukon–Alaska NO_2 contrast should be interpreted as a persistent satellite-observed column pattern rather than as direct evidence of proportional differences in surface exposure or emissions.

3.2. Seasonal patterns

Seasonal composites show persistent jurisdictional contrasts (Table 2). For CO, AK exceeds YT in every season by ~5–11% (AK/YT ratio: winter = 1.10, spring = 1.09, summer = 1.05, fall = 1.11), with the seasonal amplitude modest in both regions (max–min: YT ≈ 0.0030 mol m^{-2}; AK ≈ 0.0027 mol m^{-2}). Confidence bounds indicate stability: for example, CO 95% CIs are narrow within seasons (e.g., AK spring 0.03187-0.03533 vs YT spring 0.02903−0.03251), with only slight overlap in spring and clear separation in winter and fall. For NO_2, YT remains an order of magnitude higher than AK across all seasons (YT/AK ratio: winter ≈ 5.4×; spring ≈ 13.7×; summer ≈ 14.6×; fall ≈ 9.7×). Seasonal modulation is stronger in YT (summer-winter amplitude ≈ 4.6×10^{-5} mol m^{-2}, ~1.7 × change) than in AK (≈ 1.1×10^{-6} mol m^{-2}, ~29% change), while 95% CIs remain tight relative to means (e.g., YT summer 6.95×10^{-5}–7.46×10^{-5}), reinforcing the robustness of these contrasts over 2019–2024.

3.3. Monthly patterns

Monthly composites and their cross-year summaries confirm persistent jurisdictional contrasts with seasonally modulated gaps (Tables 3 and 4). For CO, AK exceeds YT in most months, with

Table 1
Pollutant average annual concentration in the jurisdictions of Yukon and Alaska

Average Amount	Year	YT	AK	Graphical Results
CO (mol/m2)	2019	0.0309	0.0331	
	2020	0.0293	0.0326	
	2021	0.0310	0.0340	
	2022	0.0271	0.0296	
	2023	0.0301	0.0319	
	2024	0.0295	0.0320	
	Statistics			
	x̄	0.02965	0.03220	
	SD	0.00143	0.00149	
	UCL (95%)	0.03115	0.03376	
	LCL (95%)	0.02815	0.03064	
NO_2 (mol/m2)	Year	YT	AK	
	2019	4.84e-05	5.05e-06	
	2020	4.83e-05	4.06e-06	
	2021	4.65e-05	4.01e-06	
	2022	4.91e-05	4.62e-06	
	2023	5.18e-05	4.38e-06	
	2024	4.89e-05	3.81e-06	
	Statistics			
	x̄	4.88e-05	4.32e-06	
	SD	1.72e-06	4.58e-07	
	UCL (95%)	5.06e-05	4.80e-06	
	LCL (95%)	4.70e-05	3.84e-06	

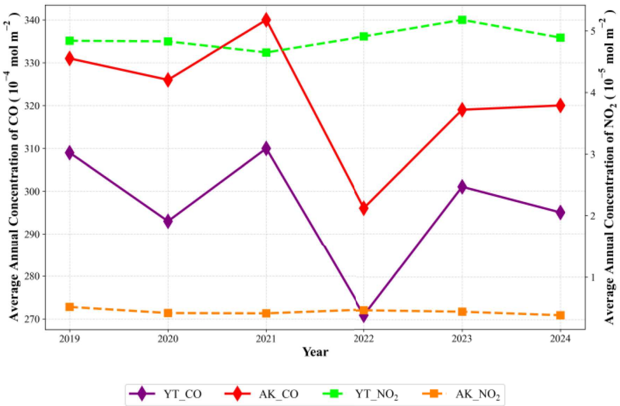

Note: (1) x̄: the arithmetic average of the six annual values (2019–2024); (2) SD: the sample standard deviation; (3) UCL (95%): upper 95% confidence limit; (4) LCL (95%): lower 95% confidence limit.

Table 2
Seasonal concentration of CO and NO_2 for Yukon and Alaska from Winter 2019 to Fall 2024

		Season							
		YT				AK			
Average amount	Year	Winter	Spring	Summer	Fall	Winter	Spring	Summer	Fall
CO (mol/m^2)	2019	0.0316	0.0325	0.0323	0.0276	0.0345	0.0347	0.0343	0.0300
	2020	0.0300	0.0325	0.0262	0.0288	0.0326	0.0354	0.0297	0.0320
	2021	0.0317	0.0317	0.0310	0.0298	0.0346	0.0351	0.0335	0.0334
	2022	0.0296	0.0294	0.0265	0.0236	0.0325	0.0326	0.0281	0.0260
	2023	0.0274	0.0288	0.0343	0.0292	0.0300	0.0316	0.0322	0.0328
	2024	0.0290	0.0297	0.0311	0.0280	0.0326	0.0322	0.0320	0.0314
	Statistics								
	x̄	0.02988	0.03077	0.03023	0.02783	0.03280	0.03360	0.03163	0.03093
	SD	0.00163	0.00166	0.00324	0.00222	0.00168	0.00165	0.00234	0.00269
	UCL (95%)	0.03159	0.03251	0.03363	0.03016	0.03456	0.03533	0.03408	0.03375
	LCL (95%)	0.02817	0.02903	0.02684	0.02550	0.03104	0.03187	0.02918	0.02811
NO_2 (mol/m^2)	2019	2.48e-05	5.36e-05	7.36e-05	3.38e-05	6.17e-06	4.16e-06	5.41e-06	3.87e-06
	2020	3.03e-05	5.00e-05	7.01e-05	3.69e-05	5.86e-06	3.64e-06	4.90e-06	4.47e-06
	2021	1.72e-05	5.06e-05	7.04e-05	3.81e-05	2.94e-06	4.21e-06	4.83e-06	2.87e-06
	2022	2.48e-05	5.38e-05	7.19e-05	3.79e-05	4.52e-06	3.78e-06	5.15e-06	4.98e-06
	2023	3.03e-05	5.55e-05	7.61e-05	3.82e-05	5.52e-06	3.74e-06	4.53e-06	2.80e-06
	2024	3.03e-05	5.13e-05	7.02e-05	3.74e-05	4.10e-06	3.45e-06	4.83e-06	4.05e-06
	Statistics								
	x̄	2.63e-05	5.25e-05	7.21e-05	3.71e-05	4.85e-06	3.83e-06	4.94e-06	3.84e-06
	SD	5.20e-06	2.15e-06	2.40e-06	1.66e-06	1.23e-06	2.98e-07	3.03e-07	8.68e-07
	UCL (95%)	3.17e-05	5.47e-05	7.46e-05	3.88e-05	6.14e-06	4.14e-06	5.26e-06	4.75e-06
	LCL (95%)	2.08e-05	5.02e-05	6.95e-05	3.53e-05	3.56e-06	3.52e-06	4.62e-06	2.93e-06

Note: (1) x̄ : the arithmetic average of the six interannual seasonal values (2019–2024); (2) SD: the sample standard deviation; (3) UCL (95%): upper 95% confidence limit; (4) LCL (95%): lower 95% confidence limit.

the largest differences in mid-winter to early spring: in January, the six-year monthly means are 0.03216 (AK) versus 0.02823 (YT) mol m^{-2} (AK/YT ≈ 1.14; non-overlapping 95% CIs from Table 4: AK 0.03050–0.03383, YT 0.02680–0.02965) and in March 0.03512 versus 0.03198 (≈ 1.10; CIs 0.03307–0.03718 vs 0.02989–0.03407). The gap narrows and can briefly invert during midsummer when variability peaks: July means are 0.03162 (AK) versus 0.03224 (YT), with wide, overlapping CIs (AK 0.02919–0.03405; YT 0.02681–0.03767) and larger SDs (YT 0.00517; AK 0.00232) from Table 4. Month-by-month trajectories by year (from Table 3) show the lowest CO means in June for both jurisdictions (YT 0.02657; AK 0.02851, per Table 4). For NO_2, YT exhibits a clear warm-season maximum and winter minimum in the cross-year summaries: June 7.73×10^{-5} (95% CI 7.39×10^{-5}–8.07×10^{-5}) versus January 2.48×10^{-5} (1.78×10^{-5}–3.17×10^{-5}), while AK remains an order of magnitude lower with modest modulation, peaking near August/January (AK 5.68×10^{-6}; 5.11×10^{-6}–6.25×10^{-6} and 5.22×10^{-6}; 3.66×10^{-6}–6.78×10^{-6}) and reaching a monthly minimum in March (3.17×10^{-6}; 2.72×10^{-6}–3.61×10^{-6}), all from Table 4. December values for YT are unavailable after QA screening (see Table 3) and are omitted from the monthly summaries.

3.4. Spatial hotspot patterns

The spatial distribution of CO concentrations (Figure 2) reflects consistent hotspots in both YT and AK across 2019–2024. Very High CO levels are dominant in the northern parts of YT, particularly along the Arctic coast plain near Old Crow, whereas the south near Whitehorse exhibits predominantly Very Low to Low concentrations. The 2019–2024 data display High and Very High CO concentrations fluctuating yearly in central YT, with 2023 showing the largest readings of Very High. A reduction occurs in 2022, wherein Moderate concentrations occupy previous High zones, but northern hotspots persist. AK demonstrates varying patterns as Very High concentrations occur in interior regions (Fairbanks) and the western coast (Bethel), while the south and east (Wrangell) near YT display Very Low to Low levels. Both territories exhibit year-to-year fluctuations in hotspot intensity; both locations' concentrations peak in 2019, and they both register troughs in 2022. This suggests similar regional-scale atmospheric processes influence CO distribution patterns across transboundary regions.

The spatial distribution of NO_2 concentrations (Figure 3) demonstrates pronounced geographical patterns in both regions, with repeated hotspots found in specific locations. In YT, Very High and High relative NO_2 concentrations repeat along the northern boundaries (Arctic Coastal Plain near Old Crow and the Porcupine River basin), particularly between 2022 and 2024, while in the south and center (Whitehorse, Watson Lake valley, and Carmacks–Pelly Crossing corridor), Very Low to Moderate values predominantly prevail. AK has more complex spatial heterogeneity, in which the highest values are massed in south-central regions (Anchorage and the Kenai Peninsula), while the

Table 3
Jurisdiction-wide monthly composites of (a) CO and (b) NO_2 column density (mol m^{-2}) for YT and AK, January 2019-December 2024

Average Amount	Month	Jurisdiction											
		YT						AK					
		2019	2020	2021	2022	2023	2024	2019	2020	2021	2022	2023	2024
CO (mol/m2)	1	0.029480	0.027942	0.030217	0.027570	0.026567	0.027577	0.032797	0.031798	0.034518	0.031870	0.029649	0.032354
	2	0.033627	0.031968	0.033205	0.031665	0.028212	0.030350	0.036213	0.035272	0.036163	0.034045	0.030988	0.033294
	3	0.034503	0.034037	0.032550	0.030373	0.030043	0.030382	0.037142	0.037116	0.036412	0.033512	0.033435	0.033119
	4	0.032594	0.032918	0.033046	0.030645	0.028952	0.030696	0.035280	0.035983	0.036142	0.033457	0.031792	0.033409
	5	0.030342	0.030577	0.029526	0.027329	0.027340	0.028048	0.031812	0.033198	0.032718	0.030851	0.029455	0.030100
	6	0.028298	0.025638	0.025850	0.026365	0.025922	0.027351	0.029632	0.028380	0.028080	0.028985	0.027077	0.028886
	7	0.034225	0.026637	0.029707	0.028834	0.041191	0.032851	0.035283	0.029254	0.031317	0.029096	0.032704	0.032052
	8	0.034330	0.026346	0.037348	0.024200	0.035695	0.033200	0.038130	0.031455	0.041239	0.026203	0.036884	0.034954
	9	0.029079	0.027013	0.032656	0.023401	0.030090	0.029416	0.031142	0.029884	0.036713	0.025510	0.033446	0.032904
	10	0.026763	0.029889	0.029367	0.023764	0.029526	0.028521	0.029578	0.033120	0.032432	0.026163	0.033877	0.031908
	11	0.026884	0.029591	0.027326	0.023636	0.027926	0.026163	0.029301	0.033130	0.031046	0.026439	0.031161	0.029410
	12	-	-	-	-	-	-	0.030848	0.033009	0.031476	0.029236	0.032163	0.031461
NO_2 (mol/m2)	1	2.25E-05	2.90E-05	1.34E-05	2.35E-05	2.78E-05	3.23E-05	6.38E-06	4.31E-06	4.80E-06	5.18E-06	7.41E-06	3.24E-06
	2	2.71E-05	3.15E-05	2.10E-05	2.61E-05	3.29E-05	2.84E-05	5.95E-06	5.23E-06	3.88E-06	4.67E-06	5.27E-06	2.40E-06
	3	3.55E-05	3.37E-05	3.80E-05	4.10E-05	4.32E-05	3.53E-05	3.94E-06	3.10E-06	2.74E-06	3.03E-06	3.29E-06	2.89E-06
	4	5.46E-05	5.01E-05	4.82E-05	5.25E-05	5.63E-05	5.15E-05	4.01E-06	3.09E-06	4.72E-06	3.21E-06	3.27E-06	3.13E-06
	5	7.06E-05	6.62E-05	6.54E-05	6.80E-05	6.70E-05	6.70E-05	4.52E-06	4.71E-06	5.16E-06	5.10E-06	4.67E-06	4.33E-06
	6	8.14E-05	7.42E-05	7.35E-05	7.65E-05	8.05E-05	7.79E-05	4.45E-06	3.66E-06	3.04E-06	4.15E-06	1.65E-06	5.10E-06
	7	7.59E-05	7.44E-05	7.45E-05	7.57E-05	7.95E-05	7.13E-05	6.14E-06	4.86E-06	6.26E-06	5.49E-06	5.62E-06	4.44E-06
	8	6.35E-05	6.16E-05	6.33E-05	6.36E-05	6.83E-05	6.15E-05	5.63E-06	6.19E-06	5.17E-06	5.83E-06	6.30E-06	4.95E-06
	9	4.86E-05	4.92E-05	5.11E-05	4.88E-05	5.25E-05	4.90E-05	5.30E-06	5.30E-06	4.28E-06	4.97E-06	4.05E-06	4.07E-06
	10	3.51E-05	3.15E-05	3.88E-05	3.55E-05	3.74E-05	3.38E-05	3.39E-06	3.49E-06	4.16E-06	4.23E-06	2.60E-06	3.73E-06
	11	1.77E-05	2.99E-05	2.44E-05	2.92E-05	2.46E-05	2.94E-05	2.92E-06	4.63E-06	1.80E-07	5.76E-06	1.75E-06	4.34E-06
	12	-	-	-	-	-	-	8.02E-06	1.32E-07	3.71E-06	3.89E-06	6.67E-06	3.14E-06

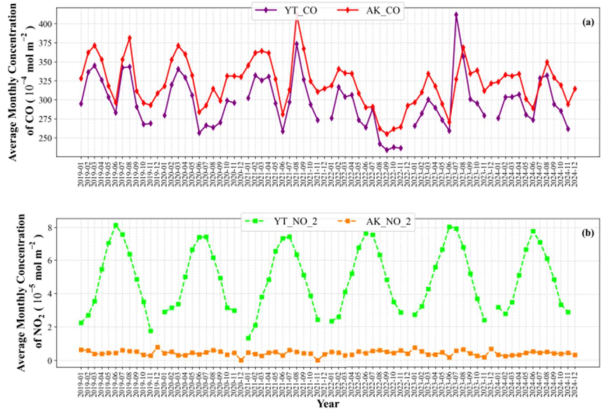

Table 4
Monthly statistical summaries of CO and NO_2 column density (mol m^{-2}) over YT and AK, aggregated across 2019–2024

		Statistics							
		YT				AK			
Average Amount	Month	x̄	SD	UCL (95%)	LCL (95%)	x̄	SD	UCL (95%)	LCL (95%)
CO mol/m^2)	1	0.02823	0.00136	0.02965	0.02680	0.03216	0.00158	0.03383	0.03050
	2	0.03150	0.00199	0.03359	0.02942	0.03433	0.00201	0.03643	0.03222
	3	0.03198	0.00199	0.03407	0.02989	0.03512	0.00196	0.03718	0.03307
	4	0.03148	0.00164	0.03320	0.02975	0.03434	0.00173	0.03616	0.03253
	5	0.02886	0.00148	0.03041	0.02731	0.03136	0.00148	0.03291	0.02981
	6	0.02657	0.00104	0.02767	0.02548	0.02851	0.00088	0.02943	0.02758
	7	0.03224	0.00517	0.03767	0.02681	0.03162	0.00232	0.03405	0.02919
	8	0.03185	0.00533	0.03744	0.02626	0.03481	0.00533	0.04040	0.02922
	9	0.02861	0.00313	0.03190	0.02532	0.03160	0.00378	0.03557	0.02763
	10	0.02797	0.00235	0.03043	0.02551	0.03118	0.00286	0.03418	0.02818
	11	0.02692	0.00198	0.02900	0.02484	0.03008	0.00227	0.03246	0.02770
	12	–	–	–	–	0.03137	0.00128	0.03271	0.03002
NO_2 (mol/m^2)	1	2.48e-05	6.63e-06	3.17e-05	1.78e-05	5.22e-06	1.49e-06	6.78e-06	3.66e-06
	2	2.78e-05	4.23e-06	3.23e-05	2.34e-05	4.57e-06	1.27e-06	5.90e-06	3.24e-06
	3	3.78e-05	3.68e-06	4.16e-05	3.39e-05	3.17e-06	4.23e-07	3.61e-06	2.72e-06
	4	5.22e-05	2.95e-06	5.53e-05	4.91e-05	3.57e-06	6.57e-07	4.26e-06	2.88e-06
	5	6.74e-05	1.81e-06	6.93e-05	6.55e-05	4.75e-06	3.25e-07	5.09e-06	4.41e-06
	6	7.73e-05	3.23e-06	8.07e-05	7.39e-05	3.67e-06	1.21e-06	4.95e-06	2.40e-06
	7	7.52e-05	2.67e-06	7.80e-05	7.24e-05	5.47e-06	7.11e-07	6.21e-06	4.72e-06
	8	6.36e-05	2.47e-06	6.62e-05	6.10e-05	5.68e-06	5.41e-07	6.25e-06	5.11e-06
	9	4.99e-05	1.57e-06	5.15e-05	4.82e-05	4.66e-06	5.97e-07	5.29e-06	4.04e-06
	10	3.53e-05	2.59e-06	3.81e-05	3.26e-05	3.60e-06	5.97e-07	4.23e-06	2.97e-06
	11	2.59e-05	4.70e-06	3.08e-05	2.09e-05	3.26e-06	2.06e-06	5.42e-06	1.10e-06
	12	–	–	–	–	4.26e-06	2.78e-06	7.18e-06	1.34e-06

Note: (1) x̄ : the arithmetic average of the six-monthly values (2019–2024); (2) SD: the sample standard deviation; (3) UCL (95%): upper 95% confidence limit; (4) LCL (95%): lower 95% confidence limit.

northern Arctic coast (Prudhoe Bay and Deadhorse) has Very Low values despite hosting the largest oil field in North America. Over time, YT's northern hotspots expanded spatially to Very High purple zones, but only in values relative to respective years. AK demonstrates relatively stable High orange-red zones around urban corridors, whereas Low to Moderate NO_2 concentrations are consistent across the remainder of the State. The data reveal NO_2 levels are much higher in YT than AK, suggesting divergent atmospheric pollution dynamics between these adjacent northern regions. Because the hotspot maps are based on Jenks classification rather than inferential cluster testing, the Very Low–Very High categories should be interpreted as relative burden classes for screening and visualization, not as statistically confirmed hotspot clusters.

3.5. Comparison of satellite observations with emission inventories and limited ground-monitoring data

The satellite–inventory comparisons (Figure 4) show highly variable strengths of association between pollutants and jurisdictions. These comparisons are intended as unit-independent concordance assessments rather than validation exercises because satellite column densities (mol m^{-2}) and inventory-based emissions estimates represent different physical quantities and are influenced by distinct atmospheric and reporting processes. CO comparisons have weak but positive correlation for both territories ($R^2 \approx 0.04$ for YT, $R^2 \approx 0.17$ for AK), with moderately greater correlation in AK. NO_2 measurements exhibit greater variability: The strongest association was observed for YT NO_2 (negative relationship; $R^2 \approx 0.24$), whereas no comparable AK NO_2 monitoring dataset was available for empirical comparison during the study period. Conducting these analyses as unit-independent concordance assessments rather than direct validation exercises enables practical interpretation in data-sparse Arctic environments. The objective is not to infer emissions from satellite observations but rather to evaluate whether independent evidence streams exhibit broadly consistent directional patterns. In this context, satellite observations serve as complementary monitoring tools that provide extensive spatial coverage and help prioritize locations where additional monitoring, inventory review, or field investigation may be warranted.

Figure 2
CO spatial distribution covering the 2019–2024 period for Yukon (a)–(f) and Alaska (g)–(l)

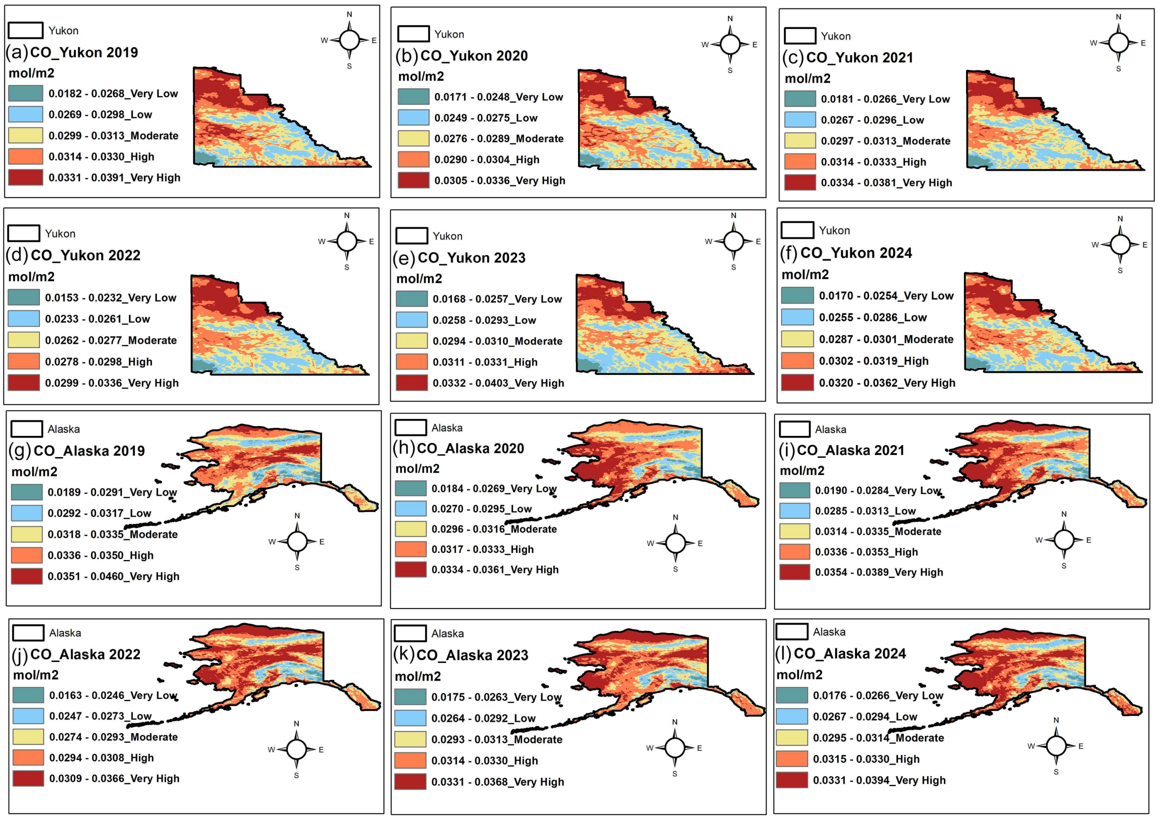

Figure 3
NO_2 spatial distribution covering the 2019–2024 period for Yukon (a)–(f) and Alaska (g)–(l)

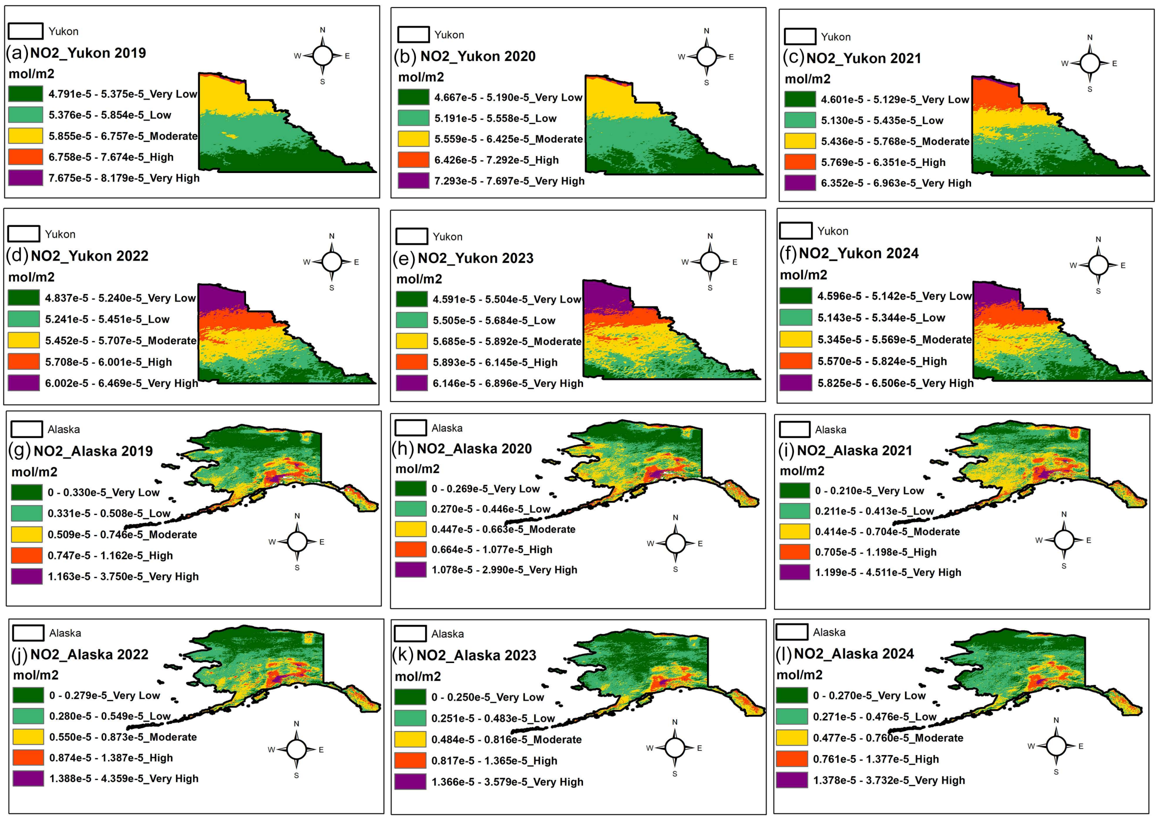

Figure 4

Scatter plots showing unit-independent concordance assessments between annual satellite-derived pollutant column densities and jurisdiction-level emission inventories or available monitoring datasets during 2020–2023: (a) Yukon CO, (b) Alaska CO, and (c) Yukon NO_2. These comparisons are presented as exploratory evidence of directional consistency rather than validation of emissions or surface concentrations

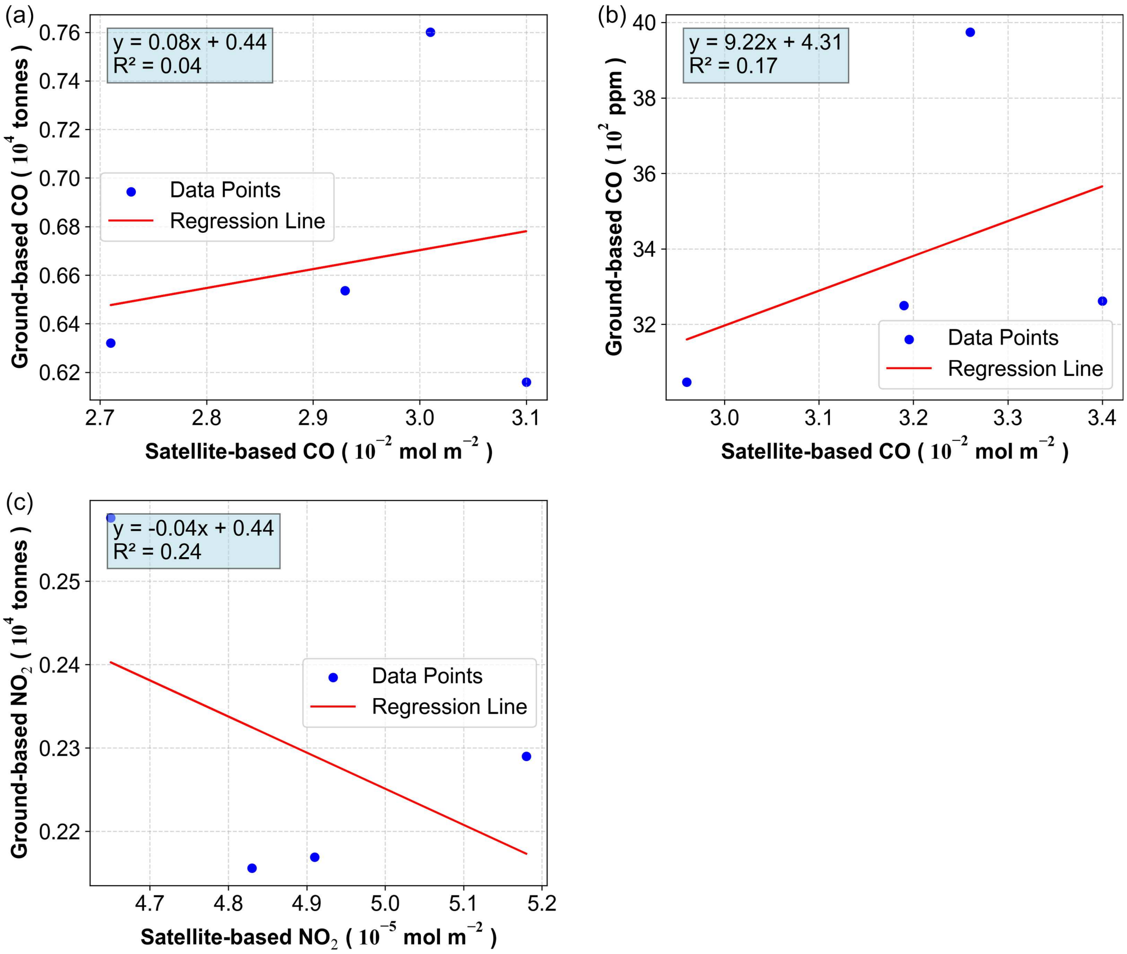

3.6. Nonparametric trend testing and slope estimation

Table 5 summarizes MK tests for annual series (n = 6) and SMK tests for monthly series (YT: n = 66; AK: n = 72) for CO and NO_2 during 2019–2024. At the annual scale (MK), no monotonic trends are detected for CO or NO_2 in either jurisdiction (all $p \geq 0.27$), reflecting limited power over six years. At the monthly scale (SMK), CO declines significantly in both regions at roughly ~1.5% per year (YT: p = 0.03; AK: p = 0.004). For NO_2, monthly SMK tests indicate no significant trend in either YT (p = 0.16) or AK (p = 0.08), with effect sizes small relative to seasonal variability.

4. Discussion

This study treats Sentinel-5P observations as a screening-level decision-support tool for sparsely monitored Arctic jurisdictions. The results complement recent Arctic remote-sensing literature by showing how paired YT–AK comparisons can reveal persistent CO and NO_2 contrasts, seasonal risk windows, and candidate areas for follow-up monitoring. The contribution is therefore not a new statistical method but an integrated framework that links satellite-observed atmospheric patterns with cautious planning and interpretation for low-carbon transition and Arctic resilience.

The annual means reveal a stable jurisdiction-specific split, with AK consistently higher in CO and YT consistently higher in NO_2, indicating persistent regime differences rather than isolated anomalies (Table 1). These directions accord with Arctic–sub-Arctic assessments that link elevated CO to regional combustion and long-range transport and elevated NO_2 to localized NO_x sources and boundary-layer trapping [11, 24, 41]. We note that across 2019–2024, CO confidence ranges minimally overlap (small, persistent AK>YT difference), whereas NO_2 intervals are non-overlapping by ≈ one order of magnitude, underscoring a structural separation in the NO_x regime. This separation is large enough to anchor jurisdiction-specific management windows. The AK-higher CO pattern is consistent with other boreal regions where wildfire activity and long-range transport dominate annual CO budgets (Pacific Northwest/Western Canada; Siberia) [24, 42, 43]. Conversely, the YT-higher NO_2 resembles observations from Scandinavian mining and small-grid settings where localized combustion under stable winter boundary layers maintains elevated NO_2 baselines despite low population density [41, 44] and contrasts with stronger annual NO_2 declines reported for large mid-latitude urban regions following regulatory tightening [45, 46]. The modest interannual spread points to jurisdiction-scale persistence rather than idiosyncratic years [47]. A noteworthy

Table 5
Trend statistics from Mann–Kendall (MK) and Seasonal Mann–Kendall (SMK) tests applied to annual (n = 6) and monthly (n = 66 for YT, n = 72 for AK) CO and NO_2 time series for Yukon Territory (YT) and Alaska (AK) during 2019–2024

Test	Pollutant	Region	n	Kendall's τ	Sen's slope (mol m^{-2} yr^{-1})	% change yr^{-1}	p-value	Trend	Significance
MK	CO	YT	6	–0.2	-28×10^{-5}	–0.94	0.72	No trend	Not significant
		AK	6	–0.33	-23×10^{-5}	–0.72	0.47	No trend	Not significant
	NO_2	YT	6	0.33	3.33×10^{-7}	0.48	0.47	No trend	Not significant
		AK	6	–0.46	-1.43×10^{-7}	–3.32	0.27	No trend	Not significant
SMK	CO	YT	66	–0.24	-46×10^{-5}	–1.55	0.03	Decreasing	Significant
		AK	72	–0.3	-49×10^{-5}	–1.51	0.004	Decreasing	Significant
	NO_2	YT	66	0.16	3.33×10^{-7}	0.68	0.16	No trend	Not significant
		AK	72	–0.18	-1.33×10^{-7}	–3.08	0.08	No trend	Not significant

departure from some pan-Arctic syntheses is the steady YT NO_2 baseline despite fire and meteorological variability, implying durable local/industrial NO_x sources and winter stratification that damp expected swings [44, 48]. By holding latitude and synoptic setting nearly constant, our bilateral comparison design isolates how source mix and boundary-layer dynamics shape persistent contrasts, an advantage over pan-Arctic syntheses that pool heterogeneous regimes. From a green and low-carbon economy perspective, such persistent contrasts are useful because they help distinguish where cleaner heating, improved fuel systems, and monitoring expansion are likely to have the highest practical value. The large YT–AK NO_2 contrast should be interpreted cautiously. Although the contrast is persistent across annual, seasonal, and monthly summaries, Sentinel-5P NO_2 retrievals in high-latitude regions are sensitive to solar geometry, snow and ice reflectance, cloud screening, boundary-layer structure, and surface–column representativeness. The available inventory and monitoring comparisons are therefore insufficient to treat the contrast as a validated emissions difference or direct exposure gradient. Instead, the result should be interpreted as a robust satellite-observed column pattern that identifies where additional winter-focused ground monitoring, source-specific measurements, and retrieval validation would be most valuable.

Three mechanisms jointly explain the stable AK>YT (CO) and YT»AK (NO_2) ordering: source mix, boundary-layer physics, and fire/transport. (i) Source structure: sustained winter heating and transport activity in AK elevate CO, whereas more concentrated point/area NO_x sources (industrial/mining, diesel micro-grids) raise YT NO_2 [49, 50]. (ii) Meteorology and boundary-layer physics: frequent cold-season inversions and shallow mixed layers amplify near-surface NO_2 in populated/industrial corridors, while deeper warm-season mixing and enhanced photochemistry modulate CO and NO_2 differently [29, 51, 52]. (iii) Fire regimes and long-range transport: episodic summertime wildfires inject CO-rich plumes that, depending on residence time and ventilation, widen or narrow the AK-YT gap [43, 53]. The 2022 muted CO offers a "natural experiment": The 2022 muted CO pattern may reflect a combination of dispersion-favorable meteorological conditions, wildfire variability, and lingering post-pandemic changes in regional activity levels, although the present analysis was not designed to establish causal attribution [54, 55]. Satellite-based lockdown studies similarly reported coherent NO_2/CO/SO_2 responses at regional scale like Bangladesh [56]. Comparable dynamics in western Canada/US Pacific Northwest (CO/fire) and Scandinavian extractive belts (winter-stratified NO_2) reinforce the generality of these mechanisms [41, 42]. These mechanisms also imply that low-carbon interventions should be differentiated rather than uniform across the two jurisdictions. In practical terms, AK's higher CO burden points more strongly toward combustion-efficiency, smoke-readiness, and heating-system improvements, whereas YT's NO_2 signal suggests greater value in targeting localized diesel dependence, point-source monitoring, and cleaner distributed energy options.

When the contrasts are most informative: CO gaps are largest in Jan–Mar and tighten/occasionally invert in Jul–Aug as fire-season variance grows; YT's NO_2 shows a reproducible summer peak/winter minimum, while AK's NO_2 remains low and weakly modulated (Tables 2, 3, and 4). AK's winter-spring CO premium and midsummer variance spike match boreal North America (NWT, northern BC, Alberta's boreal belt) where heating demand, shallow cold-season mixing, and fire weather shape monthly columns [11, 24]. The summer CO crest and early-fall minimum also mirror Siberia/Yakutia wildfire seasonality [11]. YT's summer-max, winter-min NO_2 resembles Nordic Arctic remote/mining communities (Finnish/Swedish Lapland)-diesel micro-grids + summer photochemistry set the cycle, with winter inversions boosting surface NO_2 more than columns [15]. AK's small late-winter uptick (~Feb–Mar) and shallow early-summer dip (~Jun–Jul) align with coastal Greenland/Iceland and the Canadian High Arctic, where sparse urban combustion and marine/katabatic ventilation limit amplitude [57, 58]. More relevant high-latitude analogues from Norway and Finland indicate that TROPOMI NO_2 interpretation in northern settings is shaped by seasonal retrieval availability, boundary-layer mixing, and surface–column representativeness, which is consistent with the cautious interpretation adopted here [23]. Overall, the monthly patterns fit a broad Arctic–sub-Arctic template in which CO reflects heating and wildfire influences, while NO_2 reflects localized combustion, inversion dynamics, and retrieval constraints. For planning purposes, these seasonal patterns identify candidate windows for follow-up monitoring and preparedness assessment.

Figure 2 shows a repeatable CO geography: persistent Very High/High belts in interior AK (notably the Fairbanks basin and YT-Kuskokwim lowlands) and along northern YT toward the Arctic Coastal Plain near Old Crow, with Very Low–Low levels around Whitehorse and coastal/southern AK. This pattern is consistent with topographic channeling, cold-pooling, and transport corridors that favor stagnation in valley systems and interior basins (e.g., Fairbanks) while ventilating coastal/southern sectors [59, 60]. The 2019 high → 2022 trough → 2023 rebound sequence signals shared mesoscale/fire forcing across the border, paralleling recurrent stagnation zones in boreal basins [61], and the activity/dispersion dip of 2022 with fire-active 2023 [62–65]. This transboundary synchrony echoes interior-basin CO hotspots in the Mackenzie-Great Slave corridor (NT), BC interior plateaus, and West Siberian lowlands [66, 67]. For policy, these "stagnation corridors" are candidate areas for evaluating inversion-time advisories and smoke-ready health messaging. More broadly, they also provide a practical basis for prioritizing scarce investments in cleaner heating systems, indoor air protection, and seasonal preparedness infrastructure. A useful operational rule would be to trigger enhanced winter inversion response where a basin is classified as High or Very High in at least three of the previous five winters.

Figure 3 shows a durable south-central AK hotspot belt, from Anchorage through the Kenai Peninsula, consistent with the canonical coupling of NO_x to urban/industrial corridors and major road networks and with regulated yet persistent mobile/stationary sources [68–70]. This corridor logic mirrors findings from Metropolitan Tehran, where Sentinel-5P observations combined with Moran's I and LISA hotspot analyses identified persistent pollutant clustering associated with transportation activity, urban structure, and land-use patterns [71–73]. In contrast, northern YT exhibits recurrent High–Very High NO_2 along the Arctic Coastal Plain near Old Crow and the Porcupine River basin (especially 2022–2024), despite sparse population, a discrepancy pointing to diesel micro-grids, cold-season inversions in river basins, and lofted/transported NO_x reservoirs imperfectly captured by limited surface monitors [74, 75]. Meanwhile, Prudhoe Bay/Deadhorse remains comparatively low in the column product despite oil infrastructure, illustrating how marine/katabatic ventilation and vertical sensitivity of satellite retrievals can mute surface-proximate signals in coastal Arctic settings [5, 41]. Additional uncertainty may arise because satellite NO_2 retrievals can be less sensitive to highly localized industrial emissions and flaring activity in complex Arctic environments, particularly where strong ventilation and retrieval-related limitations affect column detectability. These patterns are especially relevant for low-carbon energy planning. They support winter inversion-time alerts for Anchorage-adjacent valleys, while also highlighting northern YT as a plausible priority area for diesel-to-hybrid micro-grid upgrades, cleaner local heating, and selective monitoring expansion. In remote settlements where infrastructure budgets are constrained, this type of hotspot persistence can help direct investment toward locations where emissions reduction, reliability improvement, and health protection may be achieved simultaneously.

Figure 4 shows that column-surface relationships are directionally informative but heterogeneous, as expected when contrasting satellite column densities with surface inventories/monitors [44]. For CO, AK exhibits the stronger association ($R^2 \approx 0.17$) relative to YT ($R^2 \approx 0.04$), consistent with more vertically mixed wildfire/transport plumes in AK and greater representativeness mismatch in YT's complex terrain and micro-grid settings [46, 47]. This urban–rural contrast mirrors Madrid's pattern, where overpass-matched Sentinel-5P NO_2 tracked in situ variability best at urban/suburban monitors [45]. For NO_2, the weak or inverted associations (negative slope in YT; no AK comparison due to missing monitoring data) likely reflect a combination of representativeness mismatch, temporal aggregation differences, and retrieval sensitivity under high-latitude conditions rather than a physically meaningful inverse emissions–concentration relationship [46, 47]. Satellite column observations integrate atmospheric burdens over broad spatial domains, whereas inventories represent estimated source emissions that may not fully capture transport, boundary-layer processes, or seasonal accumulation effects. These factors can contribute to weak or even negative empirical relationships, particularly in sparsely monitored Arctic environments. Practically, Sentinel-5P offers auditable spatial coverage to triage hotspots and target scarce field assets, especially if paired with low-cost NO_2 sensor arrays in corridors where representativeness is limiting [49–52]. We recommend reporting matching assumptions (spatial/temporal collocation) and including a short sensitivity note in Supplementary Information. From a governance perspective, the value of these comparisons is not strict validation alone but improved targeting of scarce monitoring resources. In other words, Sentinel-5P can help identify where limited ground investments, such as low-cost sensor deployment or reference-grade winter monitoring, are most needed to support accountable and cost-efficient decision-making in remote northern systems.

MK on the annual series ($n = 6$) finds no monotonic trends for either pollutant (all $p \geq 0.27$), which is expected given MK's limited power at short record lengths and variance inflation from serial correlation [52, 53]. Applying SMK to the monthly series increases power and resolves modest but significant CO declines (~1.5% year^{-1}) in both YT ($p = 0.03$) and AK ($p = 0.004$). Mechanistically, these declines are plausible and additive: (i) gradual improvements in heating/transport combustion efficiency and cleaner fuels; (ii) post-pandemic mobility/energy shifts that did not fully rebound to 2019; and (iii) a downward background CO in the free troposphere over North America [8, 18, 54]. Cross-regionally, the magnitude is comparable to mid-latitude North American CO decreases in the 2010s, albeit smaller than city-scale declines under aggressive fleet turnover [54, 55]. For NO_2, SMK detects no significant monthly trend in either YT ($p = 0.16$) or AK ($p = 0.08$). This contrasts with robust urban declines in Europe/United States but matches high-latitude contexts where (a) small, distributed diesel micro-grids and winter heating dominate emissions, (b) strong seasonal stratification/inversions inflate variance, and (c) low absolute columns plus satellite surface-sensitivity limits reduce detectability over sub-decadal windows [15, 25, 56]. Interannual wildfire variability further perturbs monthly NO_x chemistry and CO co-emission, intermittently masking weak structural changes [57]. An additional limitation is that no valid December NO_2 observations were available for YT after application of the quality-screening criteria. This reflects retrieval constraints associated with Arctic winter conditions, particularly low solar-elevation angles and persistent cloud cover, rather than an absence of atmospheric NO_2. Because these observations failed the predefined quality thresholds, they were retained as missing values rather than interpolated. Consequently, annual and seasonal summaries should be interpreted as representing quality-assured observations only, with December underrepresented in YT NO_2 analyses. Robustness note: results are stable to reasonable QA screens and (where applied) variance corrections; we recommend reporting Sen-slope 95% CIs for policy-relevant effect-size bounds. Interpreted cautiously, the declining CO signal may indicate partial progress in combustion efficiency or broader transition-related improvements, whereas the absence of a clear NO_2 trend suggests that localized sources and monitoring limitations remain unresolved.

4.1. Low-carbon planning, governance, and equity implications

The results have screening-level relevance for green and low-carbon transition in Arctic and sub-Arctic regions because they identify where atmospheric burdens, infrastructure vulnerability, and monitoring scarcity may overlap. In YT and AK, air quality is closely tied to fuel dependence, emergency preparedness, and the allocation of limited public resources. The persistent jurisdictional split suggests that transition priorities should not be assumed to be uniform across the two regions.

From a planning perspective, the main value of the framework is prioritization. Recurrent CO hotspots in interior basins and northern corridors indicate candidate areas for inversion-time response, smoke preparedness, clean-air shelter planning, and further assessment of cleaner heating options. Recurrent NO_2 hotspot patterns, particularly in northern YT and south-central AK, identify locations where diesel dependence, cleaner local heating options, hybrid micro-grid feasibility, and expanded source-specific monitoring may warrant further assessment. These interpretations should be understood as planning hypotheses rather than direct intervention prescriptions.

Operational delivery would require coupling satellite evidence with selective ground monitoring, local knowledge, and feasibility assessment. Broader Arctic monitoring initiatives, including Arctic Monitoring and Assessment Programme (AMAP)-style approaches, emphasize combining Earth observation with regional, community-based, and Indigenous-led observing programs. Tiered low-cost sensor networks, co-location with regulatory stations, and periodic QA audits could improve local representativeness in winter basins, smoke-affected corridors, and diesel-dependent settlements. A practical next step would be a two-year pilot focused on the Fairbanks–Kenai valleys and the Old Crow–Porcupine corridor, combining winter-focused monitoring, seasonal dashboards, quarterly QA review, and community participation in data interpretation.

The framework also has governance relevance, but only as a first-stage screening system. It can help identify where additional field observations, inventory review, clean-energy feasibility studies, or mitigation assessment may be most useful [4]. Because the present study does not evaluate technology costs, engineering feasibility, health outcomes, or policy effectiveness, its practical recommendations should be interpreted as monitoring priorities and planning hypotheses rather than final investment or implementation decisions.

Equity and Indigenous partnership remain central to any follow-up application. Many recurring hotspot areas overlap remote and Indigenous communities that face high energy costs, limited healthcare access, and uneven exposure burdens. Co-designed monitoring, community-owned sensor systems, clean-heat assessment, portable air-cleaning support during smoke or inversion episodes, and attention to Indigenous data sovereignty can help ensure that satellite-guided planning supports local priorities as well as technical monitoring needs.

5. Conclusion

This study suggests that Sentinel-5P can provide a first-stage, decision-support screening tool for low-carbon energy planning and Arctic air-quality resilience in sparsely monitored northern regions. Using a six-year (2019–2024), dual-pollutant, paired-jurisdiction assessment of YT and AK, the analysis identified a persistent atmospheric split: CO remained structurally higher in AK, whereas NO_2 remained substantially higher in YT. These contrasts were stable across annual and seasonal summaries, supported by recurrent hotspot patterns, and only partly modified by short-term variability. Monthly trend testing further indicated modest but significant CO declines in both jurisdictions, while NO_2 trends were not statistically detectable over the study window. The persistent YT–AK NO_2 contrast should nevertheless be interpreted cautiously because satellite-derived column differences do not directly represent proportional differences in surface concentrations or emissions and remain subject to high-latitude retrieval limitations.

The contribution of the study lies not only in documenting spatiotemporal pollutant patterns but also in translating them into evidence relevant to low-carbon transition planning. Recurrent CO burdens point to the value of smoke preparedness, inversion-time response, cleaner heating, and fuel-efficiency measures, whereas localized NO_2 hotspot patterns help identify locations where diesel dependence, distributed combustion, and corridor-specific emissions may warrant further monitoring and assessment before intervention decisions are finalized. In this way, satellite-derived air-quality evidence can serve as a first-stage screening tool for prioritizing locations where clean-heat retrofits, diesel-to-hybrid micro-grid upgrades, renewable-energy integration, monitoring expansion, and public-health interventions may be most beneficial, subject to additional site-specific investigation. More broadly, these potential follow-up actions may contribute to climate-neutral Arctic operations if supported by site-specific feasibility, cost, and community-based assessment. Because many recurring hotspot areas overlap remote and Indigenous communities facing high energy costs and limited healthcare access, co-designed monitoring and transition strategies are central to equitable Arctic resilience.

The study also has important limitations. A six-year record constrains trend power, especially for NO_2; monitoring remains asymmetric across the two jurisdictions; and column-surface comparisons are limited by representativeness differences between satellite retrievals and jurisdiction-level inventories. High-latitude retrieval challenges related to snow, ice, cloud cover, and solar geometry also remain relevant. Future work should extend the record, strengthen winter-focused validation, integrate boundary-layer and fire indicators, expand localized reference monitoring in key Arctic corridors, and evaluate air-quality dynamics alongside energy-system characteristics, infrastructure vulnerability, and socioeconomic indicators. Integration with atmospheric transport models, higher-resolution satellite products, and Indigenous-led monitoring initiatives may further improve source attribution and support adaptation planning in rapidly changing northern environments.

For YT and AK, a logical next step would be to evaluate a tiered, season-aware implementation pathway that includes inversion-response planning for interior basins, smoke-season preparedness during summer months, targeted assessment of clean-heat and diesel-to-hybrid opportunities in recurrent hotspot areas, and selective expansion of NO_2 monitoring supported by harmonized quality assurance and cross-border coordination. More broadly, the bilateral comparison framework is transferable to other high-latitude regions where climate stress, sparse monitoring, and low-carbon transition pressures are converging.

Ethical Statement

This study does not contain any studies with human or animal subjects performed by any of the authors.

Conflicts of Interest

The authors declare that they have no conflicts of interest to this work.

Data Availability Statement

Data are available from the corresponding author upon reasonable request.

Author Contribution Statement

Matthew McCarthy: Investigation, Visualization, Writing – original draft. **Davoud Ghahremanlou:** Conceptualization, Investigation, Data curation, Formal analysis, Visualization, Writing – review & editing. **Amir Ghahremanlou:** Investigation, Methodology, Conceptualization, Data curation, Software, Formal analysis, Visualization, Writing – original draft.

References

[1] Rantanen, M., Karpechko, A. Y., Lipponen, A., Nordling, K., Hyvärinen, O., Ruosteenoja, K., . . . , & Laaksonen, A. (2022). The Arctic has warmed nearly four times faster than the globe since 1979. *Communications Earth & Environment*, *3*(1), 168. https://doi.org/10.1038/s43247-022-00498-3

[2] United States National Oceanic and Atmospheric Administration. (2026). *Arctic Report Card: Update for 2025*. https://arctic.noaa.gov/report-card/report-card-2025/

[3] Stroeve, J. C., Notz, D., Dawson, J., Schuur, E. A., Dahl-Jensen, D., & Giesse, C. (2025). Disappearing landscapes: The Arctic at +2.7°C global warming. *Science*, *387*(6734), 616–621. https://doi.org/10.1126/science.ads1549

[4] Reiersen, L. O., Vorkamp, K., & Kallenborn, R. (2024). The role of the Arctic Monitoring and Assessment Programme (AMAP) in reducing pollution of the Arctic and around the globe. *Environmental Science and Ecotechnology*, *17*, 100302. https://doi.org/10.1016/j.ese.2023.100302

[5] Banaji, S. (2023). Nitrogen dioxide, carbon monoxide, natural and anthropomorphic effects, and earth's changing climate. *Atmospheric and Climate Sciences*, *13*, 62–71. https://doi.org/10.4236/acs.2023.131005

[6] Rao, S., Gutzkow, K. B., Hyllestad, S., Jore, S., Thomsen, C., Andersen, G. D., . . . , & Instanes, C. (2025). Climate change and health in the Arctic. *Scandinavian Journal of Public Health*, *53*(2), 207–214. https://doi.org/10.1177/14034948241296309

[7] Fioletov, V., McLinden, C. A., Griffin, D., Zhao, X., & Eskes, H. (2025). Global seasonal urban, industrial, and background NO_2 estimated from TROPOMI satellite observations. *Atmospheric Chemistry and Physics*, *25*(1), 575–596. https://doi.org/10.5194/acp-25-575-2025

[8] Goldberg, D. L., Nawaz, M. O., Lyu, C., He, J., Carlton, A. G., Kondragunta, S., & Anenberg, S. C. (2025). Clear-sky and cloudy-sky differences in NO_2 concentrations over the United States: Implications for satellite measurement applications. *Atmospheric Chemistry and Physics*, *25*(22), 16287–16302. https://doi.org/10.5194/acp-25-16287-2025

[9] Ghosh, A. (2026). Applications of remote sensing as climate resilience technique: A bibliometric research trends analysis. *Green and Low-Carbon Economy*, *4*(3), 281–289. https://doi.org/10.47852/bonviewGLCE32021242

[10] Jeffery, P. S., Drummond, J. R., Zou, J., & Walker, K. A. (2024). Identifying episodic carbon monoxide emission events in the MOPITT measurement dataset. *Atmospheric Chemistry and Physics*, *24*(7), 4253–4263. https://doi.org/10.5194/acp-24-4253-2024

[11] Yurganov, L., & Rakitin, V. (2022). Two decades of satellite observations of carbon monoxide confirm the increase in northern hemispheric wildfires. *Atmosphere*, *13*(9), 1479. https://doi.org/10.3390/atmos13091479

[12] Shephard, M. W., Dammers, E., Cady-Pereira, K. E., Kharol, S. K., Thompson, J., Gainariu-Matz, Y., . . . , & Zheng, Q. (2020). Ammonia measurements from space with the Cross-track Infrared Sounder: Characteristics and applications. *Atmospheric Chemistry and Physics*, *20*(4), 2277–2302. https://doi.org/10.5194/acp-20-2277-2020

[13] Chen, J., Kang, S., Wu, A., & Chen, L. (2024). Projected emissions and climate impacts of Arctic shipping along the Northern Sea Route. *Environmental Pollution*, *341*, 122848. https://doi.org/10.1016/j.envpol.2023.122848

[14] He, H., Schäfer, B., & Beck, C. (2022). Spatial heterogeneity of air pollution statistics in Europe. *Scientific Reports*, *12*(1), 12215. https://doi.org/10.1038/s41598-022-16109-2

[15] Virta, H., Ialongo, I., Szeląg, M., & Eskes, H. (2023). Estimating surface-level nitrogen dioxide concentrations from Sentinel-5P/TROPOMI observations in Finland. *Atmospheric Environment*, *312*, 119989. https://doi.org/10.1016/j.atmosenv.2023.119989

[16] Hole, G. M., Büntgen, U., Wang, Y., DeVries, B., Rees, G., & Wheeler, H. C. (2026). Dendrochronology and remote sensing reveal beaver occupancy and colonization dynamics in an expanding Arctic population. *Ecosphere*, *17*(3), e70557. https://doi.org/10.1002/ecs2.70557

[17] Mosoni, C., Hildén, M., Fronzek, S., Reyer, C. P. O., & Carter, T. R. (2024). Cross-border dimensions of Arctic climate change impacts and implications for Europe. *WIREs Climate Change*, *15*(5), e905. https://doi.org/10.1002/wcc.905

[18] Thomas, M. A., Devasthale, A., & Nygård, T. (2021). Influence of springtime atmospheric circulation types on the distribution of air pollutants in the Arctic. *Atmospheric Chemistry and Physics*, *21*(21), 16593–16608. https://doi.org/10.5194/acp-21-16593-2021

[19] Hosseini, S. Z., Raofi, R., Hamidkhaniha, S., Daneshgar, F., & Wynn, M. (2025). Green infrastructure for sustainable urban development: A case study from Tehran. *Green and Low Carbon Economy*. https://doi.org/10.47852/bonviewGLCE52025029

[20] Gibson, M. D., Heal, M. R., Li, Z., Kuchta, J., King, G. H., Hayes, A., & Lambert, S. (2013). The spatial and seasonal variation of nitrogen dioxide and sulfur dioxide in Cape Breton Highlands National Park, Canada, and the association with lichen abundance. *Atmospheric Environment*, *64*, 303–311. https://doi.org/10.1016/j.atmosenv.2012.09.068

[21] Holloway, T., Miller, D., Anenberg, S., Diao, M., Duncan, B., Fiore, A. M., . . . , & Zondlo, M. A. (2021). Satellite monitoring for air quality and health. *Annual Review of Biomedical Data Science*, *4*(1), 417–447. https://doi.org/10.1146/annurev-biodatasci-110920-093120

[22] Grzybowski, P. T., Musiał, J. P., & Markowicz, K. M. (2025). Spatial representativeness of NO_2 monitoring stations with respect to Sentinel-5P satellite based estimates. *Remote Sensing Applications: Society and Environment*, *39*, 101682. https://doi.org/10.1016/j.rsase.2025.101682

[23] Schneider, P., Hamer, P. D., Kylling, A., Shetty, S., & Stebel, K. (2021). Spatiotemporal patterns in data availability of the sentinel-5P NO_2 product over urban areas in Norway. *Remote Sensing*, *13*(11), 2095. https://doi.org/10.3390/rs13112095

[24] Schneider, S. R., Lee, K., Santos, G., & Abbatt, J. P. (2021). Air quality data approach for defining wildfire influence: Impacts on PM2. 5, NO_2, CO, and O_3 in Western Canadian cities. *Environmental Science & Technology*, *55*(20), 13709–13717. https://doi.org/10.1021/acs.est.1c04042

[25] Manos, E., Witharana, C., & Liljedahl, A. K. (2025). Permafrost thaw-related infrastructure damage costs in Alaska are projected to double under medium and high emission scenarios. *Communications Earth & Environment*, *6*(1), 221. https://doi.org/10.1038/s43247-025-02191-7

[26] Reid, K. A., Reid, D. G., & Brown, C. D. (2022). Patterns of vegetation change in Yukon: Recent findings and future research in dynamic subarctic ecosystems. *Environmental Reviews*, *30*(3), 380–401. https://doi.org/10.1139/er-2021-0110

[27] Campbell, P. C., Tong, D., Tang, Y., Baker, B., Lee, P., Saylor, R., . . . , & Qu, Z. (2021). Impacts of the COVID-19 economic slowdown on ozone pollution in the U.S.. *Atmospheric Environment*, *264*, 118713. https://doi.org/10.1016/j.atmosenv.2021.118713

[28] Jalali, A., Walker, K. A., Strong, K., Buchholz, R. R., Deeter, M. N., Wunch, D., . . . , & Drummond, J. R. (2022). A comparison of carbon monoxide retrievals between the MOPITT satellite and Canadian high-Arctic ground-based NDACC and TCCON FTIR measurements. *Atmospheric Measurement Techniques*, *15*(22), 6837–6863. https://doi.org/10.5194/amt-15-6837-2022

[29] Ye, L., & Wang, Y. (2020). Long-term air quality study in Fairbanks, Alaska: Air pollutant temporal variations, correlations, and $PM_{2.5}$ source apportionment. *Atmosphere*, *11*(11), 1203. https://doi.org/10.3390/atmos11111203

[30] Mittal, H., & Kushwaha, O. S. (2024). Policy implementation roadmap, diverse perspectives, challenges, solutions towards low-carbon hydrogen economy. *Green and Low-Carbon Economy*. https://doi.org/10.47852/bonviewGLCE42021846

[31] Vinco, E., Morrison, N., Bourassa, J., & Lhermie, G. (2023). Climate policy and Canadian crop production: A qualitative study of farmers' attitudes and perceptions towards nitrous oxide reductions. *Journal of Cleaner Production*, *418*, 138108. https://doi.org/10.1016/j.jclepro.2023.138108

[32] Anderson, J., Rode, D., Zhai, H., & Fischbeck, P. (2021). Reducing carbon dioxide emissions beyond 2030: Time to shift U.S. power-sector focus. *Energy Policy*, *148*, 111778. https://doi.org/10.1016/j.enpol.2020.111778

[33] Ghahremanlou, A., & Ghahremanlou, D. (2025). Managing methane concentrations in western Canada: Climate actions towards a net-zero target. *International Journal of Remote Sensing*, *46*(23), 9330–9348. https://doi.org/10.1080/01431161.2025.2580780

[34] Khan, S., Ouadou, A., Song, X., & Scott, G. J. (2025). High-resolution ground NO_2 estimation at hyperlocal level using deep learning with Sentinel-2 and Sentinel-5P data. *Remote Sensing Applications: Society and Environment*, *41*, 101819. https://doi.org/10.1016/j.rsase.2025.101819

[35] Yukon Bureau of Statistics. (2025). *Population Report, Q1 2025*. https://yukon.ca/en/population-report-q1-2025

[36] United States Census Bureau. (2026). *Population and Housing Unit Estimates*. https://www.census.gov/programs-surveys/popest.html

[37] Nunez, Y., Benavides, J., Shearston, J. A., Krieger, E. M., Daouda, M., Henneman, L. R., . . . , & Kioumourtzoglou, M. A. (2024). An environmental justice analysis of air pollution emissions in the United States from 1970 to 2010. *Nature Communications*, *15*(1), 268. https://doi.org/10.1038/s41467-023-43492-9

[38] Patel, A., Mallik, C., Chandra, N., Patra, P. K., & Steinbacher, M. (2024). Revisiting regional and seasonal variations in decadal carbon monoxide variability: Global reversal of growth rate. *Science of the Total Environment*, *909*, 168476. https://doi.org/10.1016/j.scitotenv.2023.168476

[39] Ghahremanlou, A., & Ghahremanlou, D. (2025). Detailed analysis of air pollution in the Canadian prairie region: A step toward net-zero emission. *Science of the Total Environment*, *963*, 178492. https://doi.org/10.1016/j.scitotenv.2025.178492

[40] Ghahremanlou, A., Ghahremanlou, D., & Burrows, D. (2026). Continental-scale spatiotemporal assessment of atmospheric methane over Australia: Hotspot persistence and priority-area screening. *Atmospheric Environment*, *375*, 121992. https://doi.org/10.1016/j.atmosenv.2026.121992

[41] Im, U., Christensen, J. H., Nielsen, O. K., Sand, M., Makkonen, R., Geels, C., . . . , & Brandt, J. (2019). Contributions of Nordic anthropogenic emissions on air pollution and premature mortality over the Nordic region and the Arctic. *Atmospheric Chemistry and Physics*, *19*(20), 12975–12992. https://doi.org/10.5194/acp-19-12975-2019

[42] Marey, H. S., Drummond, J. R., Jones, D. B., Worden, H., Clerbaux, C., Borsdorff, T., & Gille, J. (2024). A comparative analysis of satellite-derived CO retrievals during the 2020 wildfires in North America. *Journal of Geophysical Research: Atmospheres*, *129*(22), e2023JD039876. https://doi.org/10.1029/2023JD039876

[43] Mokhov, I. I., Bondur, V. G., Sitnov, S. A., & Voronova, O. S. (2020). Satellite monitoring of wildfires and emissions into the atmosphere of combustion products in Russia: Relation to atmospheric blockings. *Doklady Earth Sciences*, *495*(2), 921–924. https://doi.org/10.1134/S1028334X20120089

[44] Custard, K. D., Thompson, C. R., Pratt, K. A., Shepson, P. B., Liao, J., Huey, L. G., . . . , & Montzka, D. D. (2015). The NO_x dependence of bromine chemistry in the Arctic atmospheric boundary layer. *Atmospheric Chemistry and Physics*, *15*(18), 10799–10809. https://doi.org/10.5194/acp-15-10799-2015

[45] Ge, X., Zhou, Z., Zhou, Y., Ye, X., & Liu, S. (2018). A spatial panel data analysis of economic growth, urbanization, and NOx emissions in China. *International Journal of Environmental Research and Public Health*, *15*(4), 725. https://doi.org/10.3390/ijerph15040725

[46] Landis, M. S., & Edgerton, E. S. (2024). Field intercomparison of continuous ambient FRM and FEM NO_2 instruments in the Athabasca Oil Sands Region, Alberta, Canada and the potential impact on ambient regulatory compliance. *Journal of the Air & Waste Management Association*, *74*(1), 11–24. https://doi.org/10.1080/10962247.2023.2279169

[47] Wu, S., Huang, B., Wang, J., He, L., Wang, Z., Yan, Z., . . . , & Du, Z. (2021). Spatiotemporal mapping and assessment of daily ground NO_2 concentrations in China using high-resolution TROPOMI retrievals. *Environmental Pollution*, *273*, 116456. https://doi.org/10.1016/j.envpol.2021.116456

[48] Candeias, C., Ávila, P., Coelho, P., & Teixeira, J. P. (2019). Mining activities: Health impacts. In J. O. Nriagu (Ed.), *Encyclopedia of environmental health* (2nd ed., pp. 415–435). Elsevier. https://doi.org/10.1016/B978-0-12-409548-9.11056-5

[49] Albertin, S., Bekki, S., Savarino, J., Brett, N., Law, K. S., Cesler-Maloney, M., . . . , & Simpson, W. (2024). Unraveling urban NO_x emission sources in polluted Arctic wintertime using NO_2 nitrogen isotopes. *Journal of Geophysical Research: Atmospheres*, *129*(20), e2024JD041842. https://doi.org/10.1029/2024JD041842

[50] Brett, N., Law, K. S., Arnold, S. R., Fochesatto, J. G., Raut, J.-C., Onishi, T., . . . , & Robinson, E. S. (2025). Investigating processes influencing simulation of local Arctic wintertime anthropogenic pollution in Fairbanks, Alaska, during ALPACA-2022. *Atmospheric Chemistry and Physics*, *25*(2), 1063–1104. https://doi.org/10.5194/acp-25-1063-2025

[51] Joyce, P. L., von Glasow, R., & Simpson, W. R. (2014). The fate of NOx emissions due to nocturnal oxidation at high latitudes: 1-D simulations and sensitivity experiments. *Atmospheric Chemistry and Physics*, *14*(14), 7601–7616. https://doi.org/10.5194/acp-14-7601-2014

[52] Wiggins, E. B., Veraverbeke, S., Henderson, J. M., Karion, A., Miller, J. B., Lindaas, J., . . . , & Randerson, J. T. (2016). The influence of daily meteorology on boreal fire emissions and regional trace gas variability. *Journal of Geophysical Research: Biogeosciences*, *121*(11), 2793–2810. https://doi.org/10.1002/2016JG003434

[53] Schneider, E., Czech, H., Popovicheva, O., Chichaeva, M., Kobelev, V., Kasimov, N., . . . , & Zimmermann, R. (2024). Mass spectrometric analysis of unprecedented high levels of carbonaceous aerosol particles long-range transported from wildfires in the Siberian Arctic. *Atmospheric Chemistry and Physics*, *24*(1), 553–576. https://doi.org/10.5194/acp-24-553-2024

[54] Filali, A., Llanes, L. S., Chaouch, A., & D'Acremont, V. (2025). International transport-related carbon footprint and traveler's profile in a travel clinic before and after COVID-19. *Electronic Journal of General Medicine*, *22*(4), em659. https://doi.org/10.29333/ejgm/16368

[55] Naderi, S., Tian, X., & An, C. (2025). Assessment of mobility trends and transportation-related emissions in Canadian cities during the post-COVID-19 pandemic period. *Environmental Systems Research*, *14*(1), 3. https://doi.org/10.1186/s40068-025-00394-7

[56] Haque, M. N., Sharif, M. S., Rudra, R. R., Mahi, M. M., Uddin, M. J., & Abd Ellah, R. G. (2022). Analyzing the spatio-temporal directions of air pollutants for the initial wave of Covid-19 epidemic over Bangladesh: Application of satellite imageries and Google Earth Engine. *Remote Sensing Applications: Society and Environment*, *28*, 100862. https://doi.org/10.1016/j.rsase.2022.100862

[57] Dekhtyareva, A., Hermanson, M., Nikulina, A., Hermansen, O., Svendby, T., Holmén, K., & Graversen, R. G. (2022). Springtime nitrogen oxides and tropospheric ozone in Svalbard: Results from the measurement station network. *Atmospheric Chemistry and Physics*, *22*(17), 11631–11656. https://doi.org/10.5194/acp-22-11631-2022

[58] Kramer, L. J., Helmig, D., Burkhart, J. F., Stohl, A., Oltmans, S., & Honrath, R. E. (2015). Seasonal variability of atmospheric nitrogen oxides and non-methane hydrocarbons at the GEOSummit station, Greenland. *Atmospheric Chemistry and Physics*, *15*(12), 6827–6849. https://doi.org/10.5194/acp-15-6827-2015

[59] Pohorsky, R., Baccarini, A., Brett, N., Barret, B., Bekki, S., Pappaccogli, G., . . . , & Schmale, J. (2025). In situ vertical observations of the layered structure of air pollution in a continental high-latitude urban boundary layer during winter. *Atmospheric Chemistry and Physics*, *25*(6), 3687–3715. https://doi.org/10.5194/acp-25-3687-2025

[60] Virkkala, A.-M., Aalto, J., Rogers, B. M., Tagesson, T., Treat, C. C., Natali, S. M., . . . , & Luoto, M. (2021). Statistical upscaling of ecosystem CO_2 fluxes across the terrestrial tundra and boreal domain: Regional patterns and uncertainties. *Global Change Biology*, *27*(17), 4040–4059. https://doi.org/10.1111/gcb.15659

[61] Lebourgeois, T., Sauvage, B., Wolff, P., Josse, B., Marécal, V., Bennouna, Y., . . . , & Thouret, V. (2024). Seasonal, regional, and vertical characteristics of high-carbon-monoxide plumes along with their associated ozone anomalies, as seen by IAGOS between 2002 and 2019. *Atmospheric Chemistry and Physics*, *24*(24), 13975–14004. https://doi.org/10.5194/acp-24-13975-2024

[62] Hua, J., Liu, S., Qi, C., Wu, S., Lee, L., Hu, X., . . . , & Zeng, Z.-C. (2025). Observing carbon monoxide and volatile organic compounds from Canadian wildfires in 2023 from FengYun-3E/HIRAS-II in a dawn-dusk sun-synchronous orbit. *Remote Sensing of Environment*, *327*, 114829. https://doi.org/10.1016/j.rse.2025.114829

[63] Kinase, T., Taketani, F., Takigawa, M., Zhu, C., Kim, Y., Mordovskoi, P., & Kanaya, Y. (2025). Long-term observations of black carbon and carbon monoxide in the Poker Flat Research Range, central Alaska, with a focus on forest wildfire emissions. *Atmospheric Chemistry and Physics*, *25*(1), 143–156. https://doi.org/10.5194/acp-25-143-2025

[64] Wang, Z., Silberman, J. A., & Corbett, J. J. (2021). Container vessels diversion pattern to trans-Arctic shipping routes and GHG emission abatement potential. *Maritime Policy & Management*, *48*(4), 543–562. https://doi.org/10.1080/03088839.2020.1795288

[65] Zhang, X., Wang, H., Liu, S., Feng, M., Wang, Y., Jiang, M., & Dong, F. (2025). Unveiling the overlooked inhibitory effects of carbon dioxide on photochemical nitrate decomposition over photoactive mineral dust. *Environmental Science & Technology*, *59*(6), 3143–3152. https://doi.org/10.1021/acs.est.4c11591

[66] Buchholz, R. R., Park, M., Worden, H. M., Tang, W., Edwards, D. P., Gaubert, B., . . . , & Magzamen, S. (2022). New seasonal pattern of pollution emerges from changing North American wildfires. *Nature Communications*, *13*(1), 2043. https://doi.org/10.1038/s41467-022-29623-8

[67] Tomshin, O., & Solovyev, V. (2022). Features of the extreme fire season of 2021 in Yakutia (Eastern Siberia) and heavy air pollution caused by biomass burning. *Remote Sensing*, *14*(19), 4980. https://doi.org/10.3390/rs14194980

[68] Bertazzon, S., Couloigner, I., & Underwood, F. E. (2019). Spatial land use regression of nitrogen dioxide over a 5-year interval in Calgary, Canada. *International Journal of Geographical Information Science*, *33*(7), 1335–1354. https://doi.org/10.1080/13658816.2019.1578885

[69] Hajny, K. D., Kaeser, R., Starn, T. K., Stirm, B. H., Brockway, N., Peterson, P. K., . . . , & Shepson, P. B. (2025). Measurements of the emission rates of nitrogen oxides and greenhouse gases from the Prudhoe Bay oil field. *Journal of Geophysical Research: Atmospheres*, *130*(15), e2024JD041963. https://doi.org/10.1029/2024JD041963

[70] Müller, I., Erbertseder, T., & Taubenböck, H. (2022). Tropospheric NO_2: Explorative analyses of spatial variability and

impact factors. *Remote Sensing of Environment*, *270*, 112839. https://doi.org/10.1016/j.rse.2021.112839

[71] Ghahremanlou, A., Saffarzadeh, M., Naderan, A., & Javanshir, H. (2022). Investigating the impact of accessibility on land use and its role in environmental pollution in Tehran. *International Journal of Transportation Engineering*, *9*(4), 833–854. https://doi.org/10.22119/ijte.2021.312105.1596

[72] Ghahremanlou, A., Ghahremanlou, D., & Saady, N. M. C. (2026). Topographic friction and spatial equity: A fuzzy RS–GIS accessibility assessment of metropolitan Tehran. *Papers in Applied Geography*, 1–20. https://doi.org/10.1080/23754931.2026.2657351

[73] Ghahremanlou, A., & Ghahremanlou, D. (2026). Identifying the causes of air pollution in the Tehran Metropolis-Iran and policy recommendations for sustainability. *Aerosol Science and Engineering*, *10*(3), 370–384. https://doi.org/10.1007/s41810-025-00303-6

[74] Kerr, G. H., Goldberg, D. L., Emma Knowland, K., Keller, C. A., Oladini, D., Kheirbek, I., . . . , & Anenberg, S. C. (2022). Diesel passenger vehicle shares influenced COVID-19 changes in urban nitrogen dioxide pollution. *Environmental Research Letters*, *17*(7), 074010. https://doi.org/10.1088/1748-9326/ac7659

[75] Raut, J. C., Law, K. S., Onishi, T., Daskalakis, N., & Marelle, L. (2022). Impact of shipping emissions on air pollution and pollutant deposition over the Barents Sea. *Environmental Pollution*, *298*, 118832. https://doi.org/10.1016/j.envpol.2022.118832

How to Cite: McCarthy, M., Ghahremanlou, D., & Ghahremanlou, A. (2026). Sentinel-5P Evidence for Low-Carbon Energy Planning and Arctic Air-Quality Resilience in Yukon and Alaska. *Green and Low-Carbon Economy*. https://doi.org/10.47852/bonviewGLCE62029684